

Segregation of B, P, and C in the Ni-Based Superalloy, Inconel 718

TALUKDER ALAM, PETER J. FELFER, MAHESH CHATURVEDI,
LEIGH T. STEPHENSON, MATTHEW R. KILBURN, and JULIE M. CAIRNEY

Small additions of B, P, and C can result in dramatic changes in the mechanical performance and welding behavior of Inconel 718. Although additions of B and P improve the mechanical properties, they have a detrimental effect on weldability. Adding C mitigates the negative effect on welding while retaining the improvements in mechanical performance. In this study, precise observations of the segregation of B, P, and C to the grain boundaries are made using site-specific atom probe tomography and NanoSIMS. Changes in the segregation behavior provide a quantitative explanation for the welding response, where hot cracking is attributed to the formation of a eutectic film. Calculations of the relative positions of the B, P, and C revealed that these atoms were less likely to cluster together in the presence of C, providing insight into the likely mechanisms behind the segregation behavior in this complex, multicomponent alloy.

DOI: 10.1007/s11661-012-1085-9

© The Minerals, Metals & Materials Society and ASM International 2012

I. INTRODUCTION

INCONEL 718 (IN718) is a complex engineering material that can withstand the extreme environments experienced by jet engine components because of its excellent high temperature strength and superior corrosion and creep performance.^[1,2] Trace amount additions of boron (B) and phosphorus (P) have been reported to be beneficial in increasing the creep resistance and fatigue life of IN718.^[3-7] Because of the high cost associated with the material and production of IN718, welding is the preferred method to repair the damage suffered by the alloy while in service. Although B and P help to lengthen the service life of the alloy, they have an adverse effect on the weldability of IN718. Alloys with B and P additions suffer from microfissuring in the heat-affected zone (HAZ) near the grain boundary region during welding. The microfissuring has been attributed to segregation of minor elements to the grain boundaries, locally lowering the melting point^[8,9] or forming precipitates that may undergo constitutional liquation during welding.^[10] Recently, additions of carbon (C) have been shown to counteract this negative effect,^[11,12] decreasing the average fissure crack length significantly.

The effect of each of these minor elements (B, P, and C) individually on the behavior of Ni-based superalloys

has been investigated extensively and is well understood.^[13] B is highly beneficial for improving creep properties; additions of ~0.01 wt pct have been shown to extend rupture life by an order of magnitude and improve rupture stress by a factor of 2 to 3.^[14,15] However, a large number of studies have confirmed that microfissuring during welding increases significantly when B is present^[11,13] and increases as the amount of B is increased.^[16] P has also been shown to have a beneficial effect on the creep properties of 718 alloys.^[17] Cao and Kennedy^[18,19] reported that that optimal high-temperature properties were obtained with the addition of 0.012 wt pct B and 0.022 wt pct P, which is considerably higher than the normal concentration of B and P in Inconel 718 (30 to 50 ppm B and 3 to 5 ppm P). However, this higher B and P alloy was found to have a dramatically reduced weldability performance, with sharply increased microfissuring observed in the HAZ.^[11] C is often added to Ni-based superalloys in small amounts (0.02 to 0.15 wt pct) to form carbides, improving creep life.^[13] Although additions of <0.1 wt pct C have a minor negative effect on microfissuring,^[11] weldability is still within acceptable limits, and it is generally accepted that the benefits of C for mechanical properties far outweigh any negative effects on weldability.^[13]

Although the effect of each individual element is well understood, the interplay between multiple elements in alloys with two or more different elements has been less well characterized. In a study of the effect of minor elements on the weldability of Inconel-type superalloys, Benhadad *et al.*^[12] demonstrated that the addition of 220 ppm P to the 110 ppm B had a dramatic negative effect, increasing the average total crack length per section (average TCL) to about 300 μm compared to only around 20 μm in the base alloy. However, the addition of 0.033 wt pct C to this B- and P-rich alloy substantially reduced the average TCL to a much more acceptable value of ~80 μm . They proposed that C

TALUKDER ALAM and PETER J. FELFER, Ph.D. Students, LEIGH T. STEPHENSON, Research Associate, and JULIE M. CAIRNEY, Associate Professor, are with the Australian Centre for Microscopy and Microanalysis, The University of Sydney, Sydney, NSW 2006, Australia. Contact e-mail: julie.cairney@sydney.edu.au MAHESH CHATURVEDI, Professor, is with the Department of Mechanical and Industrial Engineering, The University of Manitoba, Winnipeg, MB R3T 5V6, Canada. MATTHEW R. KILBURN, Associate Professor, is with the Centre for Microscopy, Characterisation and Analysis (CMCA), The University of Western Australia, Crawley, WA 6009, Australia.

Manuscript submitted May 15, 2011.

Article published online March 16, 2012

prevents P or B from segregating to the grain boundary either by preferentially occupying sites located at the grain boundary or by binding them in the carbides in the vicinity of the grain boundary (for B). Data adapted from References 14 and 11 that demonstrates the improvements in stress rupture life provided by the addition of minor elements is shown in Figure 1(a), and the effect of the same combinations of elements on the welding performance is shown in Figure 1(b).

In this report, we investigate systematically the role of C in mitigating the negative effects of B and P during welding. Atom probe tomography and NanoSIMS analysis (CAMECA SAS, Gennevilliers, France) were used to quantitatively study the segregation behavior of B, P, and C at the grain boundaries. For atom probe tomography, data were obtained from specifically selected high angle boundaries to study the segregation effects. Atom probe tomography data sets from the matrix were investigated also to measure the extent of aggregation or “clustering” of the minor elements to determine whether insights about the segregation behavior can be gleaned from the arrangement of the solute atoms in the matrix.

II. EXPERIMENTAL

The samples investigated in this study are known as WE91 (0.006 wt pct C) and G727 (0.033 wt pct C). These alloys are variants of IN718 with similar trace additions of B and P, which differ only in their C concentration. The composition of the two alloys is listed in Table I. The alloys were solution treated at 1323 K (1050 °C) for 30 to 45 minutes and water quenched.

SIMS analyses were carried out on the samples with a CAMECA NanoSIMS 50. The samples were embedded in Wood’s metal and polished to attain a flat surface. A 16 keV Cs⁺ primary ion beam was used to sputter ions from the sample surface. Prior to each measurement, the surface was cleaned with a high-energy primary ion beam.

The mass spectrometer was tuned to detect the ion species ¹²C⁻, ¹⁶O⁻, ¹¹B¹⁶O⁻, ³¹P⁻, and ⁵⁸Ni⁻. The choice

of using the ¹¹B¹⁶O⁻ signal on mass 27 was necessitated by the fact that the ¹¹B⁻ signal on mass 11 and the ¹¹B¹⁶O₂⁻ signal on mass 43 were too low to be detected. As a result of potential isobaric interferences, careful cross referencing was carried out to ensure that the signal was indeed ¹¹B¹⁶O⁻. The ²⁷Al⁻ peak was easily resolvable, but it was impossible to resolve potential overlaps from the ¹²C¹⁵N⁻ and ¹³C¹⁴N⁻ peaks, which sit either side of the BO peak. Cross referencing the mass 27 image with the ¹²C¹⁴N⁻ signal and the ¹²C⁻ signal confirmed that there was no contribution from C or N on the ¹¹B¹⁶O⁻ peak. The peak positions for ¹²C⁻, ¹⁶O⁻, and ⁵⁸Ni⁻ were calibrated on the Inconel samples. The ³¹P⁻ peak position was calibrated using the ³⁰Si¹H⁻ peak on Si wafer, and the ¹¹B¹⁶O⁻ peak position calibrated using the ²⁷Al⁻ and ¹²C¹⁵N⁻ peaks on different materials.

Images of the grain boundaries were acquired from a 20 × 20-μm field of view, 256 × 256 pixels, with a beam current of 0.5 pA, a dwell time of 45 ms/pixels, and a ~80-nm primary beam diameter. Image processing was

Table I. Composition of the Two IN718 Alloys (Values are in wt pct Except Where Denoted)

Element	WE91	G727
C	0.006	0.033
Mo	2.89	2.85
Cr	17.78	17.94
Fe	18.1	19.27
Nb	5.46	5.13
Ti	1	0.93
Al	0.54	0.59
Si	—	0.01
Ni	54.224	53.247
S*	6	5
P*	220	220
B*	110	120
Mg*	14	—
N*	63	17

*Values in ppm.

The bold font is used to highlight the elements of importance in this study.

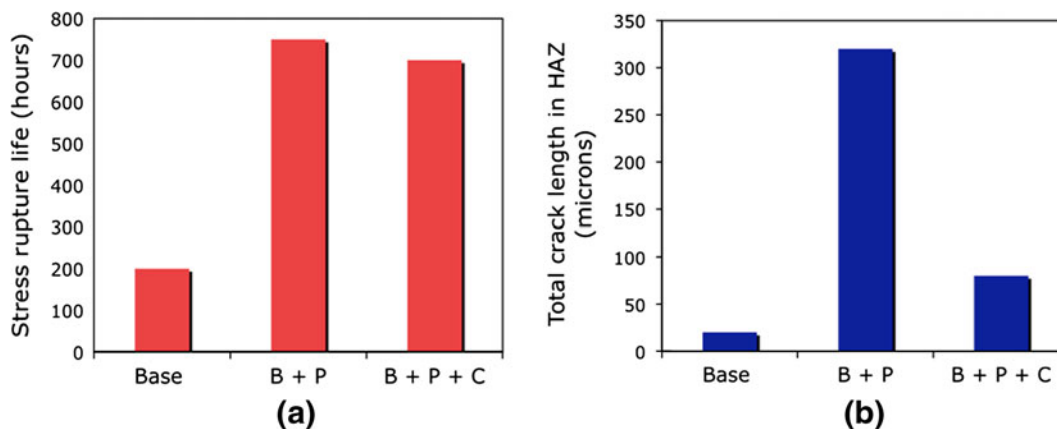


Fig. 1—(a) Stress rupture life of IN718. Adapted from Kennedy *et al.*^[14] (b) Total crack length in the HAZ in IN718. Adapted from Benhadad *et al.*^[11]

carried out using ImageJ software (U.S. National Institutes of Health, Bethesda, MD), using the OpenMIMS plugin (National Resource for Imaging Mass Spectrometry, Harvard University, Cambridge, MA), to extract deadtime-corrected data from linear profiles drawn onto the images. The correction for detector deadtime was applied to each pixel in the images using a custom ImageJ script prior to drawing line profiles. The data in the images and the line profiles are normalized to $^{58}\text{Ni}^-$ to remove any artefacts generated from the analyzed surface acting as a “getter” for any oxygen present, varying the $^{16}\text{O}^-$ signal across the image.

Bulk atom probe specimens were prepared using standard electropolishing techniques.^[20,21] Site-specific grain boundary specimens were prepared using a focused ion beam-based lift-out technique developed by the authors especially for the fabrication of grain boundary specimens.^[22] This method involves a first stage of preparation, where a rod is lifted out and attached to a sectioned and electropolished transmission electron microscope (TEM) grid and then annular milled at low keV to form a sharp needle. The specimen is then examined in a TEM to determine the precise location of the boundary before the final stage of preparation, in which low kV milling is used to position the boundary within the ~100-nm radius tip apex.

Atom probe data were collected with an Imago LEAP3000XSi (Imago Scientific Instruments, Madison, WI) operating in voltage mode at a pulsing frequency of 200 kHz. The evaporation rate was kept constant at 0.5 pct and a pulse fraction of 25 pct was used. The

temperature and flight length were set at 40 K (–233 °C) and 125 mm, respectively, for data collection from the bulk. The flight length was reverted to 90 mm for data collection from the grain boundary region. Reconstruction and visualization of the atom probe data was performed using the commercial software IVAS (Imago Scientific Instruments). A clustering analysis was carried out using the “Core Linkage” algorithm developed by Stephenson *et al.*^[23] Gibbsian interfacial excess values were calculated from cumulative diagrams (sometimes referred to as the ladder method, see for example Reference 24) using a custom MATLAB (MathWorks Inc., Natick, MA) script.

III. RESULTS AND DISCUSSION

The solution-treated alloys are expected to be homogeneous and precipitate free (no γ' or γ''). This was confirmed in a previous study^[25] by both selected-area diffraction in a transmission electron microscope and visualization of atom probe data, which showed a uniform composition for all elements. Other previous studies have shown that, with rapid cooling from solution heat-treatment temperatures by quenching, a significant portion of the B and P remains in the γ matrix.^[26]

NanoSIMS images taken from the two samples are shown in Figure 2. In these images, the intensity of each individual pixel represents the ratio of B, P, or C to Ni. The Ni content was the same in both the alloys, and no

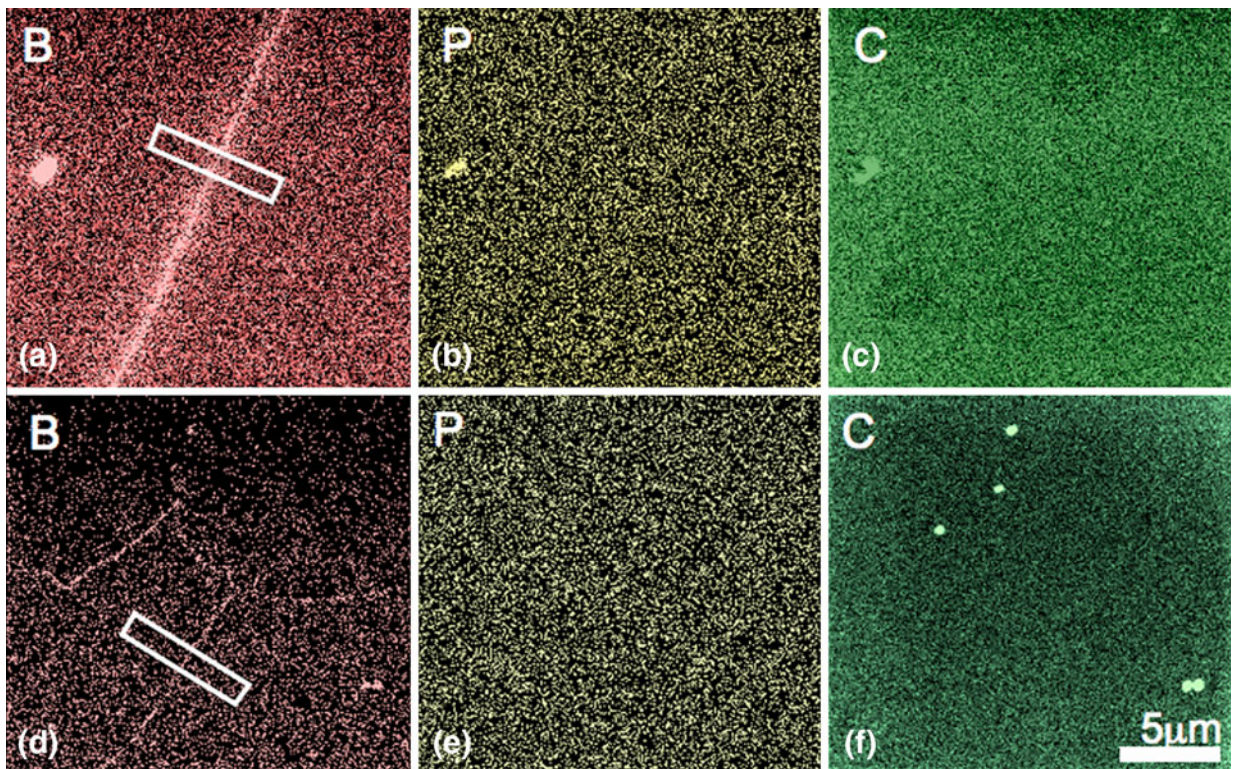


Fig. 2—SIMS images showing the ratio of B, P, or C to Ni in the WE91 (B+P) (a through c) and G727 (B+P+C) (d through f) alloys. All the images were acquired from an area of 20 μm by 20 μm .

laves phases were present that might affect the Ni count. B segregation was observed in both samples, although it was reduced significantly in the C-containing sample (G727). No segregation of P or C could be detected in the grain boundary, indicating that any segregation of these elements is below the detection limit of the NanoSIMS under these conditions. A plot showing the B-to-Ni ratio across the boundary in the areas marked in Figures 2(a) and (d) is presented in Figure 3. The dramatic decrease in the B segregation in the C-containing G727 sample is evident.

Clearly, the addition of C has a strong influence on the segregation of B to the grain boundaries. However, the NanoSIMS data do not show the behavior of C and P clearly. The atom probe is used to provide additional information. An ion-beam-generated secondary electron image showing the grain boundary areas that were prepared for examination (marked X) is shown in Figure 4(a). An atom probe specimen with the grain boundary at the tip, immediately prior to probing, is shown in Figure 4(b). Because it has been shown that previously the level of segregation varies between twin

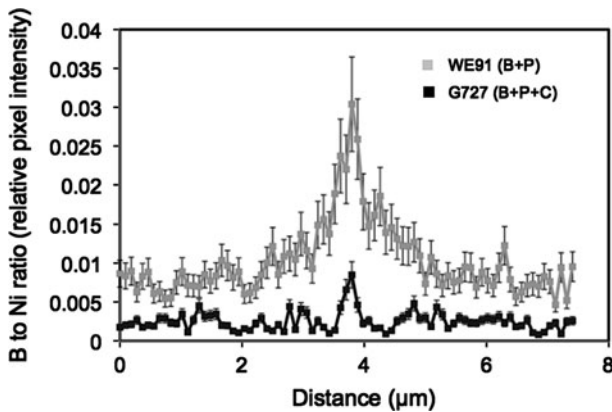


Fig. 3—B-to-Ni ratio across the grain boundaries labeled in the SIMS images shown in Fig. 2. The error bars are estimated from the variations observed when the data set is acquired from different locations along the interface.

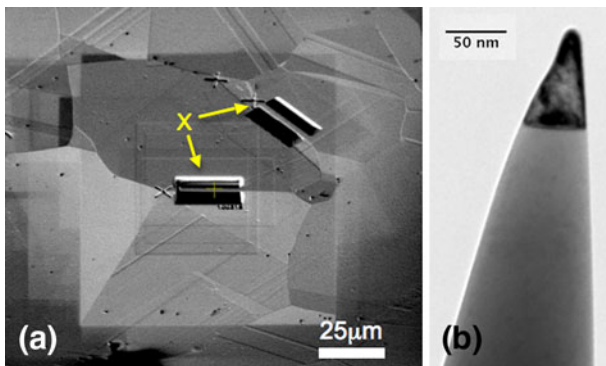


Fig. 4—(a) Ion-beam-generated secondary electron image showing the grain boundary areas that were prepared for examination (marked X), taken during the specimen preparation prior to lift out. Care was taken to avoid twin boundaries. (b) A TEM image of an atom probe tip containing the grain boundary ready for probing.

and high angle boundaries (with less segregation in the former than the latter),^[27] care was taken to avoid twin boundaries by selecting boundaries that did not seem completely flat.

Figure 5 shows the B, P, and C atoms in a reconstructed three-dimensional atom probe map for each of the two alloys. The Al atoms are also shown as light blue dots in these images. In the WE91 (B + P), a very large amount of B segregation to the grain boundary is observed, along with significant P segregation. Even in this low C alloy (0.006 wt pct), a small amount of C segregation can still be observed. In the G727 (B + P + C), the atom probe maps show clearly the lower B segregation in this alloy. P segregation is again observed, along with a significant amount of C segregation. Figures 6(a) and (b) show a compositional profile through the length of a cylindrical volume that passes perpendicularly through the each grain boundary, as shown in the inset image in these figures. A 0.5-nm step size through this volume was used. With this data, we can compare more carefully the level of grain boundary segregation. These data confirm that the WE91 (B + P) alloy has a large amount of B segregation, significant P segregation, and a small, but significant amount of C segregation. The G727 (B + P + C) grain boundary has a similar amount of P segregation and a lot less B, but the difference in the level of C is difficult to ascertain from this plot. These results are broadly consistent with previous atom probe observations of grain boundary segregation in Ni-based superalloys (many of which are reviewed in References 28 and 29), including IN718.^[20,30,31]

Although significant P segregation can be observed in the atom probe data, it is interesting to note that P was not detected by the NanoSIMS. Although SIMS is highly sensitive to small changes in concentration (it can detect down to parts per million in element imaging), it has more limited spatial resolution, especially when scans are taken from relatively large areas (the images shown are 20 μm across). The atom probe reveals that the spread of atoms about the interface is less than ~4 nm. The B segregation visible in Figure 2(a) is spread over a much larger area (~2 μm). It is, therefore, thought that the SIMS data provide information about low-level nonequilibrium segregation that results from the diffusion of vacancy-atom complexes toward the grain boundary, whereas the atom probe data show the segregation at the interface itself, which is driven by a combination of vacancy diffusion as a result of nonequilibrium conditions and a decrease of the interfacial free energy of the boundary when impurity atoms are present.^[32] The NanoSIMS and atom probe data are therefore showing entirely different information. The NanoSIMS images provide only the compositional profile in the larger region around the boundary, and the atom probe images show atomic-level compositional information from the boundary itself.

There is a difference in the observed spread of the solute atoms between the two atom probe data sets, with the solutes in the G727 alloy being spread over a greater distance (~4 nm compared to ~3 nm). It is possible that this effect is the result of artifacts in the atom probe data

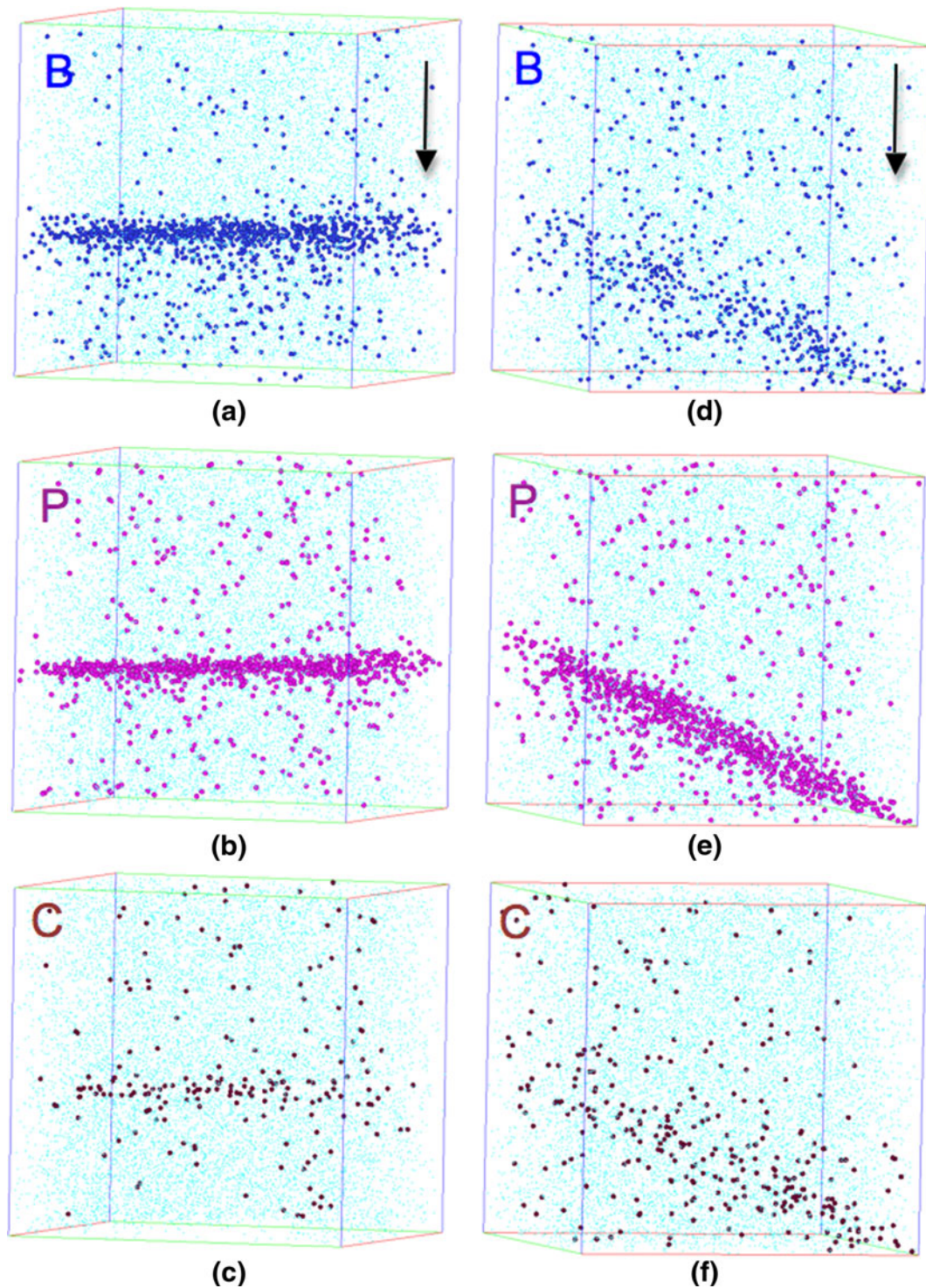


Fig. 5—Atom probe images (subset of 25 nm × 25 nm × 25 nm of the original data set) showing segregation of B, P, or C in the WE91 (B+P) (a through c) and G727 (B+P+C) (d through f) alloys. The analysis direction is marked by the arrows in (a) and (d).

because of the orientation of the grain boundaries in the data sets. It has been well established that artifacts in the measurements of segregation to grain boundaries may occur as a result of local magnification effects.^[33] These effects are minimized when the boundary is positioned normal to the direction of the analysis. The WE91 grain boundary was oriented perpendicular to the

measurement axis (the z direction), whereas the G727 boundary was misaligned by ~ 10 deg. It is, therefore, possible that the spread observed in the G727 sample arises from such local magnification effects.

An accurate quantification of the amount of segregation therefore requires careful analysis. Rather than examining the compositional profile through the

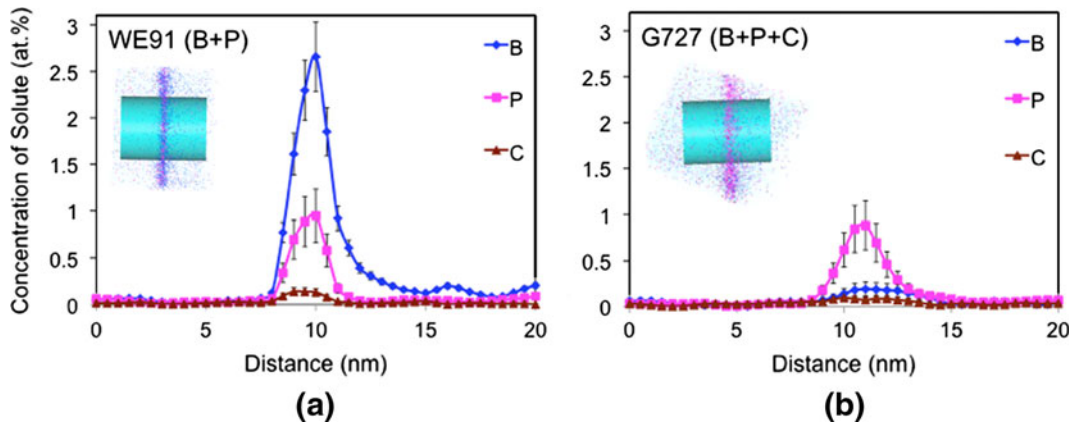


Fig. 6—Profiles showing the measured composition across a cylindrical volume of data through the grain boundaries in (a) the WE91 (B+P) alloy and (b) the G727 (B+P+C) alloy. The volume from which the data is acquired is shown inset, where the B, P, and C atoms are shown. The error bars are estimated from the variations observed when the data set is acquired from different locations along the interface.

interface, calculating the interfacial excess of solute at the interface (Γ_{solute}), which is the number of segregating atoms per unit area, allows a direct comparison between the two data sets because Γ_{solute} is not affected by local magnification effects.^[24,33] Here, the interfacial excess was calculated from cumulative diagrams (e.g., Reference 34) by summing the number of excess atoms within the grain boundary and dividing by the area of the grain boundary considered (here, 400 nm²). The values of Γ_{solute} calculated from the atom probe data for each minor element species in both alloys are shown in Figure 7. As shown previously, the large difference in the level of B segregation is apparent. The P segregation still seems to be similar, and the C segregation is enhanced in the C-containing alloy (G727) compared with the WE91.

Previous studies have attributed the role of C in mitigating the harmful effects of B and P to site competition of segregating species at grain boundaries.^[11] In their work, Benhadad *et al.*^[11] assumed that an alloy with 0.033 wt pct C contains sufficient C to compete with P and/or B for grain boundary sites, decreasing P at grain boundaries to a level where the precipitation of borides and phosphides is prevented. No evidence was found in this study to support this claim. The levels of P segregation were similar in the two alloys ($\Gamma_{\text{solute}} = 1.4$ and 1.9 atoms/nm²), and although increased C segregation was observed at the grain boundary in the C-containing G727 (a doubling of Γ_{solute} from 0.2 to 0.4 atoms/nm²), the amounts are not thought to be sufficient to lead to the large decrease in B segregation that has been observed simply through site competition.

We therefore propose that C affects the segregation behavior of B by affecting its diffusion behavior in the bulk solid solution. It has been shown that equilibrium segregation in binary systems is directly related to the solid solubility of the segregating species.^[35] The situation for multicomponent systems is much more complicated. A model proposed by Guttman^[36] for a ternary solution assumes there is a preferred interaction between the impurity and major alloying atoms present. Where a

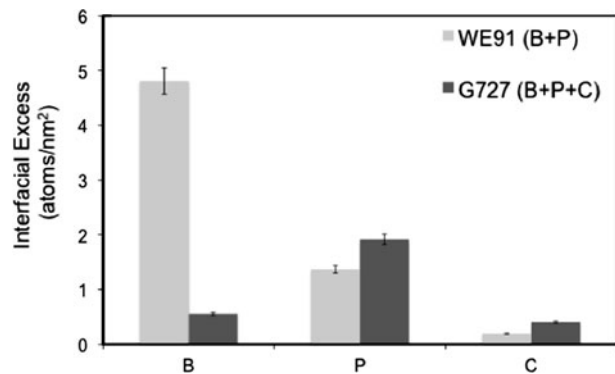


Fig. 7—The calculated interfacial excess for each of the minor elements.

preferential attraction exists between specific atoms in an alloy system (that is, where interaction coefficients are >0), synergistic equilibrium cosegregation of these atoms to interfaces or grain boundaries can occur.

To understand the precise locations of the B, P, and C atoms in the overall structure and possibly to shed some insight into the reasons for the changes in the segregation behavior between the two alloys, atom probe data from the bulk specimen were analyzed to determine whether there is any tendency for the minor elements to cluster together. These data sets were obtained from volumes that do not contain grain boundaries. The “Core Linkage” algorithm developed by Stephenson *et al.*^[23] was applied to the data sets to search for clusters. The algorithm requires the selection of two parameters, namely d_{max} and d_{link} . The value of d_{max} was optimized (selecting the value that provided the clearest indication of the deviation from random), and d_{link} was set as equal to d_{max} (note that because these values are identical, this is equivalent to using a “maximum separation” algorithm^[37]). It is also necessary to specify a minimum number of atoms for a cluster (N_{min}). Results for different values of N_{min} were compared. The analyses were limited to the minor elements (B, P, and C). For the results to be comparable, a volume of

30 nm × 30 nm × 40 nm was selected from each of the original atom probe data sets for analysis.

The percentage of the total number of P, B, and C atoms found to be contained within a cluster are shown in Figure 8(a). This plot shows results using and N_{\min} of 4, so the clusters in this plot are made up of at least four atoms of any of the three species, for example: B-B-B-B, B-P-C-B, P-P-C-C, *etc.* However, because these samples have differing solute concentrations, to compare the extent of clustering in two samples with different solute concentrations, it is necessary to consider also how many clusters would be detected if the atoms were distributed in a completely random solid solution. To achieve this, the same algorithm was used to determine the proportion of solute contained in clusters for a data set in which the atoms were labeled randomly (but having the same overall composition). The result when the number of clusters that would be expected if the atoms were distributed randomly is subtracted from the proportion of the atoms of each species that form part

of a cluster is shown in Figure 8(b). This value can be described as the extent of above-random clustering.

This analysis was performed for different values of N_{\min} to ensure that the cluster size distribution is taken into account. As would be expected, the minimum cluster size used affected the overall number of clusters measured (a lower minimum cluster size leads to more clusters being detected), but the overall trends in the extent of nonrandom clustering were the same. In this article, we present the results for a minimum cluster size (N_{\min}) of 4, as this was the lowest value for which the changes in clustering behavior could be observed with 100 pct confidence (*i.e.*, were beyond the limits of the estimated range of error calculated from the expected error in the compositional measurements).

Figure 8(b) reveals that the solute atoms are more likely to cluster together in the alloy that does not contain C (WE91) compared with the alloy that does (G727). The effect is particularly strong in the case of B, which indicates that the preferential attraction between

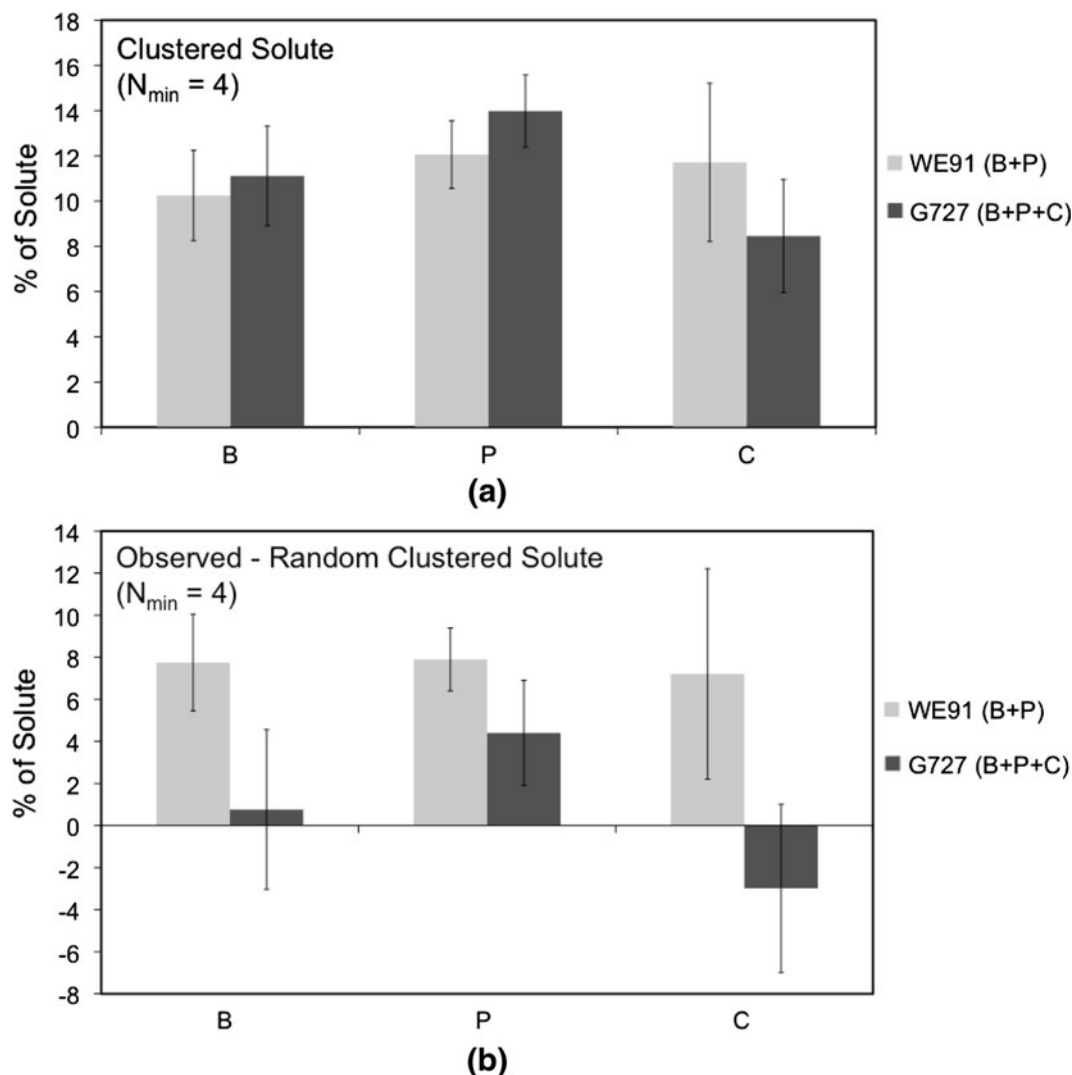


Fig. 8—(a) The proportion of the total number of B, P, or C atoms that forms part of a cluster. (b) The extent of nonrandom clustering (*i.e.*, the proportion of the atoms of each species that form part of a cluster with the number of clusters that would be expected if the atoms were randomly distributed subtracted). All values were calculated using the Core-Linkage algorithm ($N_{\min} = 4$).^[23]

B and other solute species is greater in the sample that does not contain C, consistent with the predictions by Guttman^[36,38] that, in the equilibrium case, preferential attraction (through an enhanced interaction coefficient) will lead to a greater degree of cosegregation. This equilibrium cosegregation takes place during solution treatment.

This sample is also subject to nonequilibrium segregation, which is consistent with observations by Huang *et al.*,^[39] who used SIMS to observe changes in the level of segregation of B after cooling from different temperatures that indicated that segregation occurred via a nonequilibrium mechanism when the specimen was cooled from above ~1273 K (~1000 °C). Nonequilibrium segregation occurs through the diffusion of vacancy-solute complexes during cooling, where these vacancies are annihilated at the grain boundaries. It is possible that the clusters observed reflect vacancy-solute complexes. Unfortunately, atom probe cannot provide information about vacancies within the sample. Nevertheless, the increased clustering observed in the sample that does not contain C might indicate a greater concentration of vacancy-solute complexes, which would increase the amount of cosegregated solute, consistent with our observations.

This interpretation can provide a qualitative explanation for the difference in the segregation behavior between the two alloys. In addition, the segregation data itself is precise and can provide a quantitative explanation for the difference in the welding response. Hot cracking arises if a liquid film is formed at the grain boundaries. This can happen where the local B concentration is high enough to form a thin film of Ni-Ni₃B eutectic,^[40] lowering the solidus temperature at the grain boundaries. In the presence of P, the solidus temperature is decreased possibly even more by the formation of a Ni-Ni₃B-Ni₃P ternary eutectic. Unfortunately, a ternary phase diagram is not available. The known eutectic temperatures for Ni₃P and Ni₃B are 1143 K (870 °C) and 1366 K (1093 °C)^[41] (Ni₃B is known to have a strong tendency for supercooling^[42]). The interfacial excess value for B in the low C alloy (WE91) corresponds to approximately one full monolayer of Ni₃B, whereas in the C-containing alloy (G727), it corresponds only to ~10 pct of the atoms required to form a monolayer. The amount of P in both alloys is the equivalent of ~30 pct of a monolayer. It is, therefore, concluded that hot cracking is the result of the formation of a film of eutectic in the low C alloy, significantly decreasing the local solidus temperature. In the case of the high-C alloy, the level of microfissuring is reduced significantly.

IV. CONCLUSIONS

To explain the role of C in mitigating the detrimental effects of B and P in weldability in Inconel 718, the distribution of B, P, and C was investigated in two variants of Inconel 718: WE91, which contains higher than usual amounts of B and P, and G727, which contains higher than usual amounts of B, P, and C.

NanoSIMS and site-specific atom probe tomography provided information about the segregation of each species. The information from the two techniques provided different information. NanoSIMS provided details of the segregation across a larger area away from the grain boundaries but did not resolve the fine, atomic-scale segregation to the interfaces. Atom probe provided precise, quantitative data about the segregation to the interface itself.

Quantitative data comparing the interfacial excess of the segregating species was calculated from the atom probe data. The results revealed that B segregation is reduced dramatically in the C-containing alloy (G727). In contrast, P segregation was unaffected largely by the addition of C. The improvement in welding performance in the C-containing sample (G727) is therefore attributed to the decrease in B segregation below the amount required to produce significant liquation at the grain boundaries.

C segregation was observed in both samples, even in the sample containing a low C concentration (0.006 wt pct). A larger amount of C segregation was observed in the sample with 0.033 wt pct C (G727), but this increase is not sufficient to affect the B segregation through site competition. Instead, decreased clustering of the solute atoms in the sample that contains C suggests that the addition of C changes the interaction coefficients in the matrix between the B, P, and C leading to less cosegregation. The increased clustering observed might also indicate a change in the vacancy concentration, affecting the nonequilibrium segregation behavior.

ACKNOWLEDGMENTS

This work was funded by the Australian Research Council. The authors are grateful for the scientific and technical input of the Australian Microscopy and Microanalysis Research Facility (AMMRF) nodes at the University of Sydney and the University of Western Australia and support from the AMMRF travel and access program.

REFERENCES

1. C. Sims, N. Stoloff, and W. Hagel: *Superalloys II*, John Wiley & Sons, New York, NY, 1987, pp. 3–4.
2. R.C. Reed: *The Superalloys, Fundamentals and Applications*, Cambridge University Press, Cambridge, U.K., 2006, pp. 1–2.
3. C.G. McKamey, C.A. Carmichael, W.D. Cao, and R.L. Kennedy: *Scripta Mater.*, 1998, vol. 38, pp. 485–91.
4. B.C. Yan, J. Zhang, and L.H. Lou: *Mater. Sci. Eng. A*, 2008, vol. 474, pp. 39–47.
5. Z. Hu, H. Song, S. Guo, W. Sun, and D. Lu: *J. Mater. Sci. Tech.*, 2005, vol. 21, pp. 73–76.
6. N. Li, W. Sun, Y. Xu, S. Guo, D. Lu, and Z. Hu: *Mater. Lett.*, 2006, vol. 60, pp. 2232–37.
7. L. Xiao, D.L. Chen, and M.C. Chaturvedi: *Mater. Sci. Eng. A*, 2006, vol. 428, pp. 1–11.
8. H. Guo, M.C. Chaturvedi, and N.L. Richards: *Sci. Tech. Weld. Join.*, 1999, vol. 4, pp. 257–64.
9. H. Guo, M.C. Chaturvedi, N.L. Richards, and G.S. McMahon: *Scripta Mater.*, 1999, vol. 40, pp. 383–88.

10. W.A. Owczarski, D.S. Duvall, and C.P. Sullivan: *Weld. J.*, 1966, vol. 45, pp. 145–55.
11. S. Benhadad, N. Richards, and M.C. Chaturvedi: *Metall. Mater. Trans. A*, 2002, vol. 33A, pp. 2005–17.
12. S. Benhadad, N.L. Richards, U. Prasad, H. Guo, and M.C. Chaturvedi: *Superalloys 2000*, T.M. Pollock, R.D. Kissinger, R.R. Bowman, K.A. Green, M. McLean, S. Olson, and J.J. Scbirm, eds., TMS, Warrendale, PA, 2000, pp. 703–11.
13. N.L. Richards and M.C. Chaturvedi: *Int. Mater. Rev.*, 2000, vol. 45, pp. 109–29.
14. R.L. Kennedy, W.-D. Cao, and W.M. Thomas: *Adv. Mater. Process.*, 1996, vol. 149, pp. 33–35.
15. R.F. Decker and J.W. Freeman: *Trans. Met. Soc. AIME*, 1960, vol. 218, pp. 277–85.
16. M.C. Chaturvedi, W. Chen, and A. Saranchuk: *Superalloys 718, 625, 706 and Various Derivatives*, E.A. Loria, ed., TMS, Warrendale, PA, 1997, pp. 743–51.
17. W.D. Cao and R.L. Kennedy: *Superalloys 718, 625, 706 and Various Derivatives*, E.A. Loria, ed., TMS, Warrendale, PA, 1994, pp. 463–77.
18. W.D. Cao and R.L. Kennedy: *Superalloys 718, 625, 706 and Various Derivatives*, E.A. Loria, ed., TMS, Warrendale, PA, 1997, pp. 511–20.
19. W.D. Cao and R.L. Kennedy: *Superalloys 1996*, R.D. Kissinger, D.J. Deye, D.L. Anton, A.D. Cetal, M.V. Nathal, T.M. Pollock, and D.A. Woodford, eds., TMS, Warrendale, PA, 1996, pp. 589–97.
20. D.H. Ping, Y.F. Gu, C.Y. Cui, and H. Harada: *Mater. Sci. Eng. A*, 2007, vol. 456, pp. 99–102.
21. M. Thuvander, M.K. Miller, and K. Stiller: *Mater. Sci. Eng. A*, 1999, vol. 270, pp. 38–43.
22. P.J. Felfer, S.P. Ringer, and J.M. Cairney: *Ultramicroscopy*, 2011, vol. 111, pp. 435–39.
23. L.T. Stephenson, M.P. Moody, P.V. Liddicoat, and S.P. Ringer: *Microsc. Microanal.*, 2007, vol. 13, pp. 448–63.
24. B.W. Krakauer and D.N. Seidman: *Acta Mater.*, 1998, vol. 46, pp. 6145–61.
25. T. Alam, M.C. Chaturvedi, S.P. Ringer, and J.M. Cairney: *Mater. Sci. Eng. A*, 2010, vol. 527, pp. 7770–74.
26. W. Chen, M.C. Chaturvedi, N. Richards, and G. McMahon: *Metall. Mater. Trans. A*, 1998, vol. 29A, pp. 1947–54.
27. H. Guo, M.C. Chaturvedi, and N.L. Richards: *Sci. Tech. Weld. Join.*, 1998, vol. 3, pp. 257–59.
28. D. Blavette, E. Cadel, C. Pareige, B. Deconihout, and P. Caron: *Microsc. Microanal.*, 2007, vol. 13, pp. 464–83.
29. D.N. Seidman, C.K. Sudbrack, and K.E. Yoon: *JOM*, 2006, vol. 58, pp. 34–39.
30. M.K. Miller and S.S. Babu: *Superalloys 718, 625, 706 and Various Derivatives*, E.A. Loria, ed., TMS, Warrendale, PA, 2001, pp. 357–65.
31. M.K. Miller, J.A. Horton, W.D. Cao, and R.L. Kennedy: *J. Phys. IV*, 1996, vol. 6, pp. 241–46.
32. P.E.J. Flewitt and R.K. Wild: *Grain Boundaries: Their Microstructure and Chemistry*, Wiley, Chichester, U.K., 2001, pp. 39–40.
33. D. Blavette, P. Duval, L. Letellier, and M. Guttman: *Acta Mater.*, 1996, vol. 44, pp. 4995–5005.
34. B.W. Krakauer and D.N. Seidman: *Rev. Sci. Instrum.*, 1992, vol. 63, pp. 4071–79.
35. M.P. Seah and E.D. Hondros: *Proc. Royal Soc. of London A—Mathematical and Physical Sciences*, 1973, vol. 335, pp. 191–212.
36. M. Guttman: *Surf. Sci.*, 1975, vol. 53, pp. 213–27.
37. M.K. Miller and E.A. Kenik: *Microsc. Microanal.*, 2004, vol. 10, pp. 336–41.
38. M. Guttman: *Mater. Sci. Eng.*, 1980, vol. 42, pp. 227–32.
39. X. Huang, M. Chaturvedi, and N. Richards: *Metall. Mater. Trans. A*, 1996, vol. 27A, pp. 785–90.
40. W. Chen, M.C. Chaturvedi, and N. Richards: *Metall. Mater. Trans. A*, 2001, vol. 32A, pp. 931–39.
41. T.B. Massalski, Editor-in-Chief, H. Okamoto, P.R. Subramanian, L. Kacprzak, eds: in *Binary Alloy Phase Diagrams*, 2nd ed., ASM International, Materials Park, OH, 1990.
42. K. Eckler, R.F. Cochrane, D.M. Herlach, and B. Feuerbacher: *Mater. Sci. Eng. A*, 1991, vol. 133, pp. 702–05.